Aeolian Research 31 (2018) 72–81

Contents lists available at ScienceDirect

Aeolian Research

journal homepage: www.elsevier.com/locate/aeolia

Measuring high spatiotemporal variability in saltation intensity using a low-cost Saltation Detection System: Wind tunnel and field experiments

W. de Winter[a,*], D.B. van Dam[a], N. Delbecque[b], A. Verdoodt[b], B.G. Ruessink[a], G. Sterk[a]

[a] Department of Physical Geography, Faculty of Geosciences, Utrecht University, Utrecht 3508 TC, The Netherlands
[b] Research Unit Soil Degradation and Conservation, Department of Soil Management, Ghent University, Ghent B-9000, Belgium

ARTICLE INFO

Keywords:
Aeolian transport
Saltation
Piezoelectric sensor
Wind tunnel
Field
Experiment
Spatiotemporal variability
Equal sensitivity

ABSTRACT

The commonly observed over prediction of aeolian saltation transport on sandy beaches is, at least in part, caused by saltation intermittency. To study small-scale saltation processes, high frequency saltation sensors are required on a high spatial resolution. Therefore, we developed a low-cost Saltation Detection System (SalDecS) with the aim to measure saltation intensity at a frequency of 10 Hz and with a spatial resolution of 0.10 m in wind-normal direction. Linearity and equal sensitivity of the saltation sensors were investigated during wind tunnel and field experiments. Wind tunnel experiments with a set of 7 SalDec sensors revealed that the variability of sensor sensitivity is at maximum 9% during relatively low saltation intensities. During more intense saltation the variability of sensor sensitivity decreases. A sigmoidal fit describes the relation between mass flux and sensor output measured during 5 different wind conditions. This indicates an increasing importance of sensor saturation with increasing mass flux. We developed a theoretical model to simulate and describe the effect of grain size, grain velocity and saltation intensity on sensor saturation. Time-averaged field measurements revealed sensitivity equality for 85 out of a set of 89 horizontally deployed SalDec sensors. On these larger timescales (hours) saltation variability imposed by morphological features, such as sand strips, can be recognized. We conclude that the SalDecS can be used to measure small-scale spatiotemporal variabilities of saltation intensity to investigate saltation characteristics related to wind turbulence.

1. Introduction

Coastal dunes act as a primary defense against flooding of the hinterland by the sea. The erosion of coastal dunes by storm-surges and wave motion has been studied intensively (e.g., Vellinga, 1982; Thornton et al., 2007; de Winter et al., 2015), resulting in well-developed dune-erosion models for use in scientific and applied studies (e.g., Roelvink et al., 2009; Kobayashi et al., 2009; Ruessink et al., 2012). However, the recovery rate of coastal dunes by natural aeolian transport processes on beaches is not well understood, and existing models (e.g. Durán and Moore, 2013; Keijsers et al., 2016) are predominantly exploratory. This arises from the determination that the magnitude of the maximum aeolian transport rate, predicted by empirical transport equations (e.g., Bagnold, 1941; Kawamura, 1951; Zingg, 1953; Owen, 1964; Kadib, 1965; Hsu, 1971; Lettau and Lettau, 1978; Sorensen, 2004), exceeds the maximum transport rates measured in the field (e.g., Sherman and Li, 2012; Barchyn et al., 2014) and, consequently, measured dune recovery rates are over predicted (Davidson-Arnott and Law, 1996; Keijsers et al., 2014). Besides the influence of surface characteristics (e.g. grain size, soil moisture content, surface roughness and morphology), this dissimilarity is related to wind turbulence (Stout and Zobeck, 1997).

Wind turbulence causes strongly intermittent aeolian saltation (Sterk et al., 1998; Leenders et al., 2005) when the mean wind speed is close to threshold of motion (Davidson-Arnott and Bauer, 2009). With increasing wind speed aeolian sediment transport becomes more continuous but considerable unsteadiness and hence transport intermittency remains (e.g., Stout and Zobeck, 1997; Baas and Sherman, 2005; Baas and Sherman, 2006; Baas, 2008; Davidson-Arnott and Bauer, 2009). The non-continuous flow of sediment on small spatiotemporal scales (centimeters and seconds) causes transport to be confined to a smaller amount of time and consequently affects the sediment transport rate on large timescales (Davidson-Arnott and Bauer, 2009; Barchyn et al., 2014). The demand to measure aeolian sand transport on small spatiotemporal scales is of primary interest to investigate the influence of near-bed wind turbulence on time-averaged aeolian sand transport. To measure small-scale spatiotemporal variability in sediment transport, high-frequency (1–10 Hz) saltation sensors are required

* Corresponding author.
E-mail address: w.dewinter@uu.nl (W. de Winter).

https://doi.org/10.1016/j.aeolia.2017.11.003
Received 22 February 2017; Received in revised form 2 November 2017; Accepted 10 November 2017
Available online 06 December 2017
1875-9637/

at a high spatial resolution in a horizontally oriented sensor array perpendicular to the prevailing wind direction, containing a mutual sensor distance of at least 0.10 m (Baas and Sherman, 2006).

Existing sensors that can measure saltation transport on high frequencies are based on various techniques: piezoelectric (Sensit (Stockton and Gillette, 1990), Safire (Baas, 2004), Buzzer Discs (Sherman et al., 2011), piezoelectric sensor (Raygosa-Barahona et al., 2016)), acoustic (Saltiphone (Spaan and van den Abeele, 1991; Poortinga et al., 2015), Miniphone (Ellis et al., 2009)), and laser (Wenglor Particle Counter (Hugenholtz and Barchyn, 2011; Barchyn et al., 2014; Duarte-Campos et al., 2017)). Commonly used high-frequency saltation sensors are the Saltiphone, Safire, and Sensit. The Saltiphone is an acoustic saltation sensor which can measure saltation at a temporal scale up to 16 Hz, using a microphone. Its design, containing two wind vanes at the back of the Saltiphone, ensures that the sensing area is directed into the prevailing wind direction. At the same time, this design prevents the Saltiphone from being used at a high spatial resolution, since the vanes cause the instrument to have a large (0.19 m) wind-normal span. The Safire and Sensit are both tubular sensors designed with piezo-electric technology. These instruments generate electrical pulses by converting the impact energy of particles into a particle count flux. The size and curved shape of the sensing area ensures the performance of point measurements on a high spatial resolution and omni-directional sensitivity. These sensors have the disadvantage that individual sensors show different sensitivity under seemingly identical conditions (Baas, 2004; Barchyn and Hugenholtz, 2010; Sherman et al., 2011), which makes it difficult to determine the mutual variability in saltation intensity in a multi-sensor set-up. As a result, it is required to normalize the sensor signals prior to data analysis, assuming a uniform cumulative transport rate on relatively large timescales (Baas, 2008; Lee and Baas, 2015). Furthermore, all three sensors are rather expensive, hindering high spatial resolution measurements of saltation intensity.

This paper aims to measure and analyze the spatiotemporal variability in saltation intensity on time-scales of 10 Hz with a spatial resolution of 0.10 m on a natural beach. To that end, we developed a low-cost system with multiple saltation sensors, called Saltation Detection System (SalDecS). This paper describes the technical aspects of the SalDecS, and resolves the characteristics (linearity and equal sensitivity) of the Saltation Detection sensors using wind tunnel and field measurements. In this paper we continue with a description of the physical and electronical design of the SalDecS in Section 2. The wind tunnel and field experiments are described in Section 3, followed by the results (Section 4). In Section 5 we discuss the linearity and equal sensitivity of the SalDec sensors. We finish with the conclusions in Section 6.

Fig. 1. Saltation Detection System installed at the beach. The horizontally oriented array contains 32 sensors, spaced with an interval of 0.10 m and the vertical array at the left end contains 8 sensors. A sonic anemometer is additionally present just to the right of the middle of the horizontal bar.

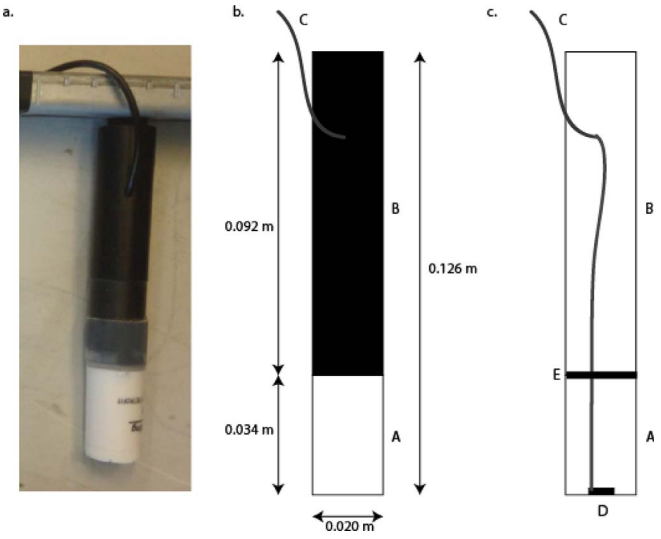

Fig. 2. Physical design of a Saltation Detection sensor, with a) photo, b) schematic exterior view and c) schematic interior view. The separate parts are A) sensor head, B) PVC-body, and C) wire to base unit, D) piezo-electric element, and E) silicone membrane.

2. Instrument description

The Saltation Detection System (SalDecS) (Fig. 1), developed and manufactured at the Department of Physical Geography of Utrecht University, The Netherlands, comprises 40 individual SalDec sensors on a carrier bar. Below, we first describe the physical design and electronics of the SalDec sensor in Sections 2.1 and 2.2, respectively. This is followed by a description of the full 40-sensor SalDecS in Section 2.3.

2.1. Physical design of the SalDec sensor

A SalDec sensor (Fig. 2) is a tubular instrument, inspired by the design of the Safire (Baas, 2004), the Buzzer Disc (Sherman et al., 2011) and the Sensit (Stockton and Gillette, 1990), and consists of a sensor head (A, Fig. 2) mounted to a tubular body of PVC with a length of 0.092 m and a diameter of 0.020 m (B, Fig. 2). The sensor head of the saltation sensor is constructed out of the PVC housing of a TL lighting starter (brand: Sylvania, type: FS-22 RAF, mean wall thickness: 7.8×10^{-4} m) and has a curved surface area with a height of 0.034 m and an outer diameter of 0.020 m. The total sensing area facing saltation transport is thus 1.07×10^{-3} m^2. Double-sided tape, with a thickness of 2.3×10^{-4} m, was used to glue a piezo-electric element (brand: Murata, type: 7bb-12-9) inside the center of the bottom of the sensor head. The nearly invariable thickness of double-sided tape enables the reproducible assembly of the piezo-electric element and sensor head, and thus an equal transfer of vibrations in every sensor. The cabling from the piezo-electric element leaves the sensor via a mounting hole in the PVC body (C, Fig. 2). To limit the detection of noise vibrations from outside the sensor head, vibrations are mechanically damped at two locations. Firstly, the sensor head is connected to the sensor body with a rubber shock absorber (brand: Saint-Gobain Performance Plastics, type: Folding Skirt Stopper DX467020-20) (E, Fig. 2). Secondly, the sensor is screwed to the carrier bar via a rubber grommet. In this way, sand grains hitting the sensor body or the carrier bar will not be detected by the piezo-electric element.

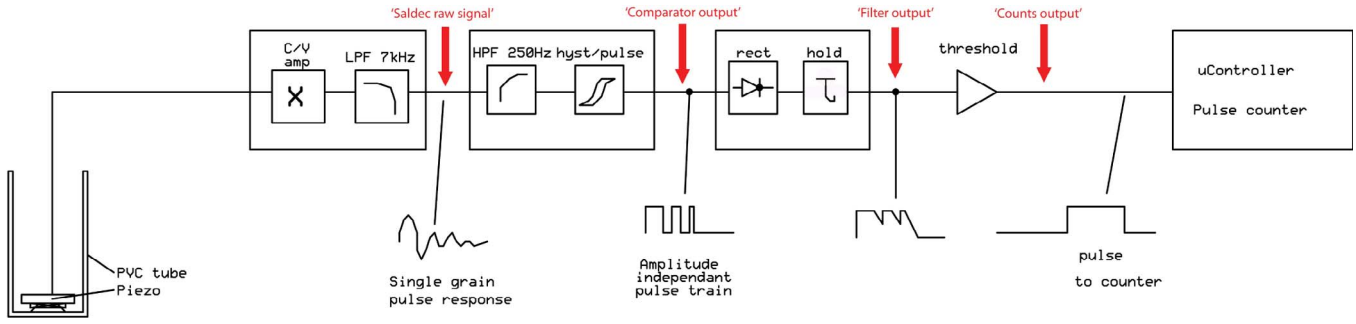

Fig. 3. Flow diagram of the electronics of the SalDecS.

2.2. Electronics

The electronics of the SalDecS are predicated on the design of the Saltiphone (Spaan and van den Abeele, 1991; Poortinga et al., 2015). The hardware is visualized as a flow diagram in Fig. 3. When a sand grain hits the sensor head, vibrations produced by the impact are transferred to the piezo-electric element. The signal produced by the piezo-electric element is processed into a pulse in three stages. In the first stage, the signal is converted into a voltage with a C/V converter. The low impedance of the input quickly dampens the vibrations of the piezo-electric element to prepare the element for subsequent impacts. Additionally, an operational amplifier (brand: Texas Instruments, type: TLV272ID) is used to filter the higher and lower frequencies from the boundaries of 8 kHz and 7 kHz, respectively. This stage results in the raw signal (Fig. 4). In the second stage, the mechanical rumble induced by the sound of wind is filtered with a first-order high-pass filter, which removes frequencies less than 250 Hz. A hysteresis, with a threshold of 2.5 mV, is used in this stage to transform the raw signal into a comparator signal (Fig. 4a). In the last stage, a 1-ms shaper (filter signal in Figs. 4b and c) is used to envelope the pulse train from the second stage hysteresis to create grain pulses with a rate up to 1 kHz (count signal in Figs. 4c and d). Thus, grain pulses with a rate up to 1 kHz can be measured. A count is registered when the count signal, created by the hysteresis, contains the transition of 'grain' to 'no grain' (in other words, the transition from 0 to 3.2 V in the count signal) within the 1-ms timeframe. When the 'grain' signal has a duration of > 0.001 s, the registration of the impact is postponed to the next 0.001-s time interval.

2.3. Description of the SalDecS

In our design, one single SalDecS contains 40 individual SalDec sensors merged on a carrier bar. The position on the carrier bar is adjustable for all sensors, but the standard mounting contains a horizontally oriented array with 32 sensors spaced at a 0.10 m interval and an additional vertically oriented array with 8 unevenly distributed sensors, spaced with mutual distances of 0.055, 0.065, 0.055, 0.065, 0.065, 0.245 and 0.140 m from bottom to top (Fig. 1, on the left-hand side of the horizontal array). The SalDec sensors are physically and electronically grouped in sets of 8 sensors, hardwired into a base unit. The base unit contains the described electronics for each sensor (Section 2.2) and is connected to an Atmel XMEGA32D4 microcontroller that counts the grain pulses of the eight sensors. Base units can be daisy chained, with a maximum of 64 units, to a central data logger. Thus, in our SalDecS design we use 5 base units (40 sensors) in every system. In total, we constructed 3 SalDecS (120 sensors) during a standardized workflow to prevent the appearance of uneven sensitivity of sensors due to manufacture. The counts detected in the microcontroller are then sent to a central data logger via an RS-485 data link. The summarized counts of the data logger are time-synchronized and are logged at a frequency of 10 Hz. A SD card is used to store the data. The cost of a 40-sensor

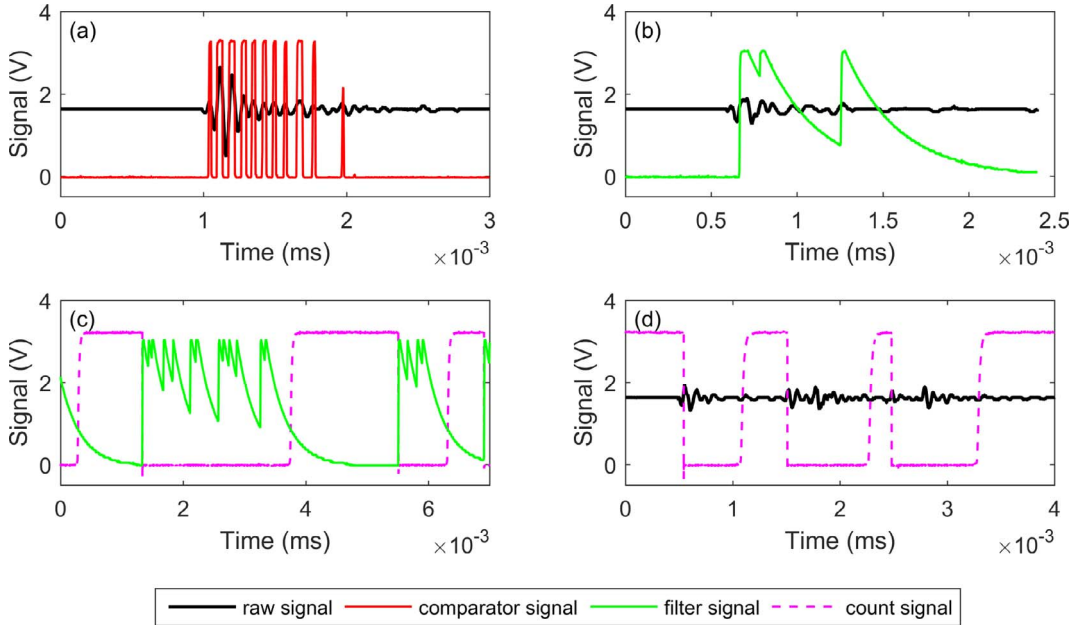

Fig. 4. Examples of the electronical signal processing of the SalDec sensors. (a) Shows a raw signal transformation into a comparator signal, (b) illustrates a filter signal resulting from the 1-ms shaper, (c) illustrates the envelopment of the filtered signal into a count signal and (d) shows the conversion of a raw signal into a count signal. Note that the signals in the individual panels are not related to each other.

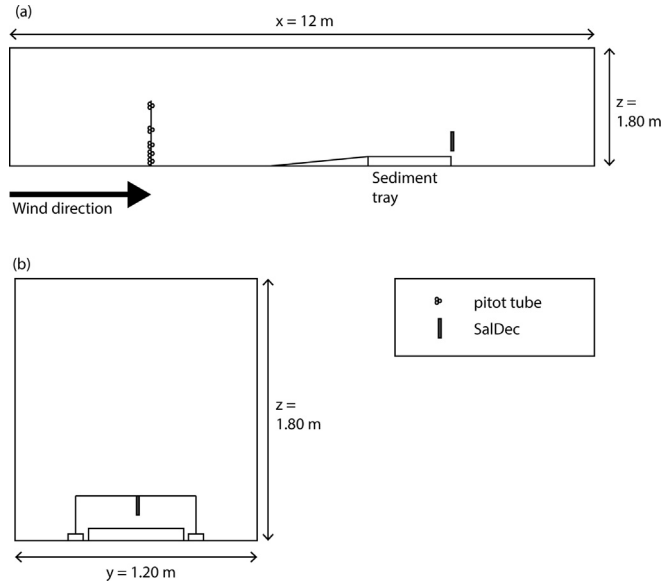

Fig. 5. Setup of wind tunnel experiments. (a) Side view of the experiment with 5 pitot tubes deployed vertically in front of the sediment tray and at the down-wind end a SalDec sensor is installed, and (b) front view of the SalDec sensor aligned on a carrier bar, 0.10 m above the down-wind end of the sediment tray.

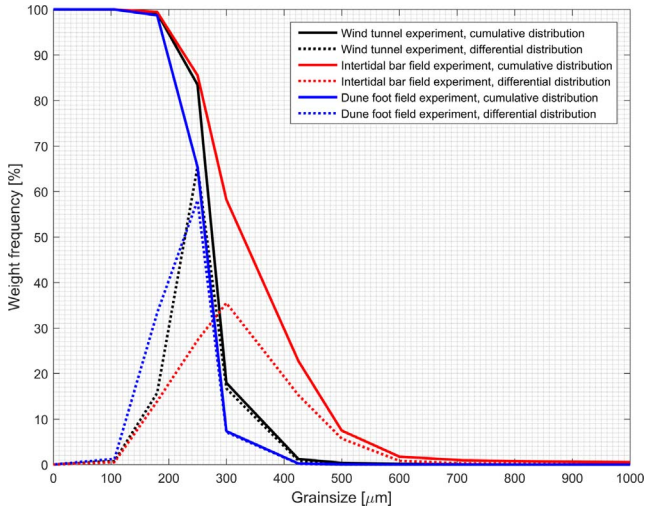

Fig. 6. Probability and cumulative probability distributions of the sand collected from the top 0.02 m layer of the surface at the dune foot and intertidal bar of our field site near Egmond aan Zee, The Netherlands. The black lines indicate the sediment used in the wind tunnel experiments and was collected on a different day (June 29, 2015) than the surface samples of the intertidal bar (red) and dune foot (blue) (October 22, 2015). The probabilities are based on the weight of sediment larger than the displayed grain sizes.

SalDecS including scaffolding and dataloggers is ~US$ 935; the average cost of one sensor is ~US$ 25. These cost are in the range of other low-cost saltation sensors such as the Miniphone (~US$ 10) (Ellis et al., 2009), the Buzzer Disc (~US$ 10) (Sherman et al., 2011) and the piezoelectric sensor of Raygosa-Barahona et al. (2016) (~US$ 50).

3. Methodology

Seven individual SalDec sensors were tested in the wind tunnel of the International Centre for Eremology at Ghent University, Belgium. Here, experiments were performed under controlled wind conditions to determine the relation between aeolian mass flux and the responding number of particle counts and sensor equality. We chose to test only 7 sensors in the wind tunnel, rather than all 120 individual sensors because conducting the experiments was time-consuming. Therefore, we conducted additional field experiments with all 120 sensors.

3.1. Wind tunnel experiments

3.1.1. Experimental setup

The working area of the wind tunnel is a chamber of 12 m in length, 1.20 m in width, and the adjustable ceiling was fixed at a height of 1.80 m (Fig. 5, upper panel; see Gabriels et al. (1997) for a complete description). Five pitot tubes were connected to Testo pressure sensors (serial number 0638.1545 for pressure sensor 1, 2, 4 and 5 and 0635.1545 for pressure sensor 3) and installed at heights of 0.038, 0.105, 0.206, 0.435, and 0.793 m (corresponding with pressure sensor number 1 up to 5) above the floor to measure the wind profile at 5.70 m down-wind from the start of the working area. To determine the mass flux, a sediment tray (1.60 m long, 0.40 m wide and 0.015 m deep) was installed between 7.80 and 9.60 m down-wind from the entry of the working area. A piece of sand paper, at the up-wind end of the sediment tray, was used to gradually increase the roughness from the wind tunnel floor to the sediment. Since the SalDec sensors are dependent on the momentum of sand grains, and thus grain size, it was decided to use sand from the field area where the SalDecS were to be deployed. The poorly graded quartz sand (D_{50} ~275 μm)(Fig. 6) was collected from the top 0.02 m of the dune foot at the beach near Egmond aan Zee, The Netherlands. The 7 sensors were selected randomly from the 120 SalDec sensors and measured at a frequency of 10 Hz. In every experiment one sensor was tested to prevent the influence of wind-normal variation in sediment transport across the sediment tray. All SalDec sensors were installed in the center of the down-wind end of the sediment tray at 0.10 m above the bed (Fig. 5, lower panel), and were exposed to 5 different wind conditions (Table 1). The wind speed at 0.90 m above the bed and the shear velocity () were derived from the experimental averaged wind velocities measured by the 5 pitot tubes using a log-linear regression of:

$$u_z = \frac{u_*}{\kappa}\ln\left(\frac{z}{z_0}\right), \quad (1)$$

where u_z is the average wind velocity (m s^{-1}) at height z (m) above the surface, is the shear velocity (m s^{-1}), κ is the Von Kármán constant (0.4) and z_0 is the roughness length (m). The wind speed varied between 9.5 and 15.5 m s^{-1} and the shear velocity ranged between 0.51 and 0.81 m s^{-1}. Due to erosion in the sediment tray, the down-wind end of the tray became barren. When barren spots became visible, the experiment was immediately stopped to avoid changes in the saltation process. Because barren spots occurred earlier in time with higher wind speeds, the duration of the experiments was dependent on the wind speed. Table 1 illustrates that experiment durations ranged from 180 s at 9.5 m s^{-1} to 105 s at 15.5 m s^{-1}. The sequence of sensors for the first wind condition was based on increasing sensor number and was reversed with every following wind condition.

3.1.2. Data processing and analysis

To determine the mass flux, the sediment tray with sand was weighed before and after every experiment. Subsequently, the mass flux was calculated by the weight difference over the width of the sediment

Table 1
Wind conditions and corresponding experiment durations.

Wind speed at 0.90 m (m s^{-1})	Shear velocity u_* (m s^{-1})	Durations (s)
9.5	0.51	180
10.5	0.56	150
12.0	0.63	135
13.6	0.67	120
15.5	0.81	105

tray divided by the duration of the experiment

$$Q = \frac{m_b - m_a}{w} \cdot \frac{1}{t}, \quad (2)$$

where Q is the mass flux (kg m^{-1} s^{-1}), m_b is the weight of the sediment tray with sediment before the experiment (kg), m_a is the weight of the sediment tray with sediment after the experiment (kg), w is the width of the sediment tray (m) which was constant in every experiment (0.40 m), and t is the duration of the experiment (s). The total number of particles counted during an experiment was divided by the duration of the experiment to determine the saltation intensity

$$I = \frac{\Sigma counts}{t}, \quad (3)$$

where I is the saltation intensity (counts s^{-1}).

3.2. Field experiments

3.2.1. Experimental setup

Field experiments were conducted on October 21 and 22, 2015 along the Holland coast, approximately 3 km south of Egmond aan Zee, The Netherlands. This relatively narrow beach (with a width of approximately 100 m during low tide) contains a bar-trough-dune morphology. During the measuring days D_{50} grain sizes of the beach surface decreased across the beach from ~330 to ~265 μm, from the intertidal bar (red in Fig. 6)) toward the dune foot (blue in Fig. 6), respectively. On October 21, 2015 saltation was measured with a frequency of 10 Hz with SalDecS 2, 3 and 4 along a down-wind array across the beach during southwesterly winds (Fig. 7, upper and lower left panel). SalDecS 2 was installed on the intertidal bar, SalDecS 3 at the dry beach down-wind of the high water line, and SalDecS 4 near the dune foot. Sand strips (Nield et al., 2011; Hage et al., under review), providing a gradual alteration of surface elevation and moisture content on a spatial scale of meters, were present above the high water line near the dune foot (Fig. 8, left, SalDecSs 3 and 4) and saltation was characterized by intermittency due to the continuous passage of streamers. On October 22, 2015 we measured saltation with the same SalDecSs, but with slower northwesterly winds (Fig. 7, upper and lower right panel). SalDecS 2 was located just on top of the bar at the transition of the intertidal bar to the intertidal channel, SalDecS 3 was aligned at the intertidal beach just down-wind from the intertidal channel, and SalDecS 4 was positioned near the dune foot. Here, sand strips were less pronounced across the beach (Fig. 8) compared to October 21. Due to the lower wind speeds, saltation transport was non-continuous in space on temporal scales of seconds to minutes as only small clouds of sand were moving across the SalDecS array occasionally. On both days, the SalDecSs were aligned perpendicular to the prevailing wind direction with the bottom of the sensors at 0.10 m above the beach surface.

3.2.2. Data analysis

We assumed that, averaged over a sufficient time period, saltation intensity must be equal in the wind-normal direction if the morphology, wind conditions and sensor sensitivity are equal. The appropriate averaging period is likely to be longer in case of strongly intermittent saltation near the initiation of motion than for more intense, nearly continuous transport. To this end, we averaged the saltation intensity over the greatest possible time period for every measuring period ranging from 0.75 h to 5.77 h (Table 2), with the largest averaging periods (>3 hours) for the low-transport day (October 22). This resulted in a time-averaged saltation intensity in counts s^{-1} for every sensor in the horizontal array of the SalDecS. Sensors with a mean value of 0 in both experiments did not operate during the experiment and were not considered for further analysis, so we analyzed 113 sensors.

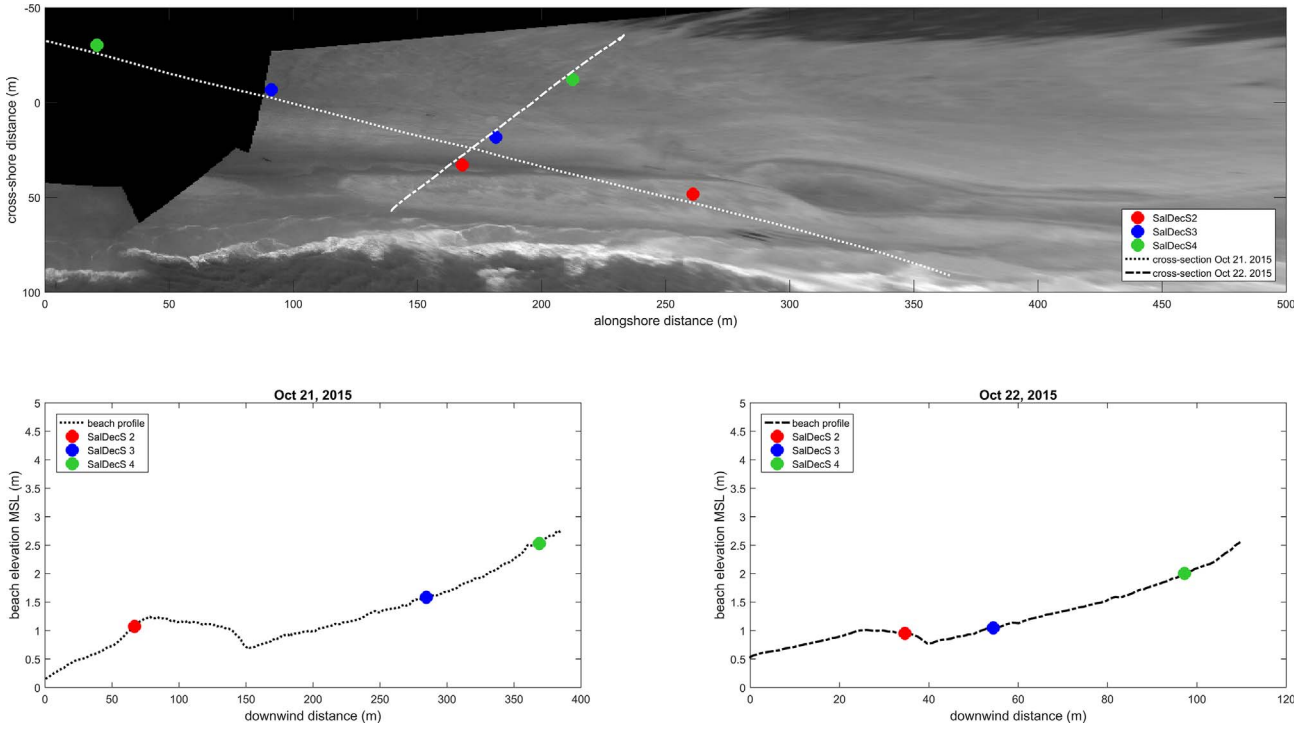

Fig. 7. Field setup on October 21 and 22, 2015. The upper panel shows the positions of the instruments and the beach profiles on a top view of the fieldwork area, with Northern direction on the left-hand side. The lower panels show the cross-sections along the down-wind distance of the instrument array for October 21 and 22, left and right, respectively. The photo of the upper panel is a rectified photograph taken from a ~50 m high tower with Argus (Holman and Stanley, 2007) video cameras (van Enckevort and Ruessink, 2001). The high intensity (white) near the bottom reflects the swash zone on the beach. Higher up, the dark alongshore band is a wet trough, while the lighter colors correspond to an (drier) intertidal bar and the upper beach toward the fore dune. The black color indicates pixels outside the camera scope.

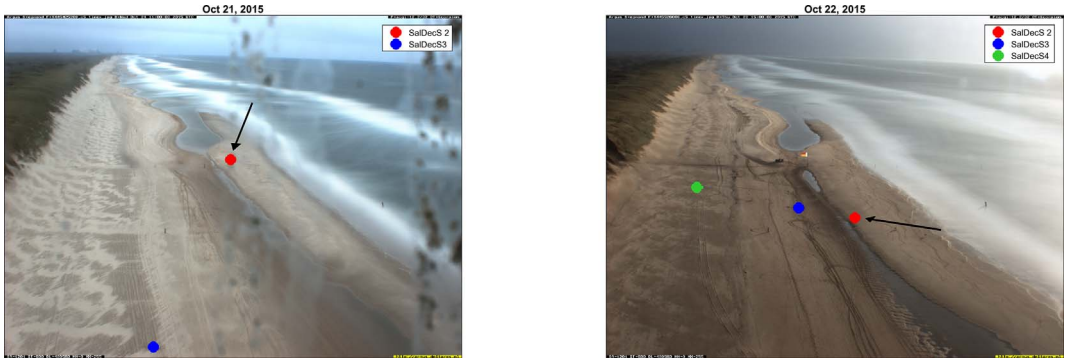

Fig. 8. Oblique top view of the fieldwork area during our measurements on October 21 (left) and 22 (right), 2015 taken by an Argus (Holman and Stanley, 2007) camera on top of a ~50 m high tower (van Enckevort and Ruessink, 2001). The arrows indicate the prevailing wind direction and the colored circles represent the locations of the three SalDecS. Note that SalDecS 4 falls outside the picture on October 21, but it was deployed near the dune foot downwind from SalDecS 3.

Table 2
Averaging time periods for field experiments.

	SalDecS (#)	Averaging period (hours)
21 Oct, 2015	2	0.75
	3	1.25
	4	1.50
22 Oct, 2015	2	3.31
	3	5.77
	4	3.73

4. Results

4.1. Wind tunnel experiments

During the wind tunnel experiments mass fluxes ranged between 0.032 and 0.202 kg m^{-1} s^{-1} and saltation intensities varied from 27.0 to 348.5 counts s^{-1}. Results show that saltation intensity increases with larger mass fluxes (Fig. 9, upper panel). The increasing trend starts linearly, but deflects with increasing mass fluxes from approximately 0.15 kg m^{-1} s^{-1}. The deflecting part of the trend shows the counted number of sand grains to be lower than expected at mass fluxes of about 0.2 kg m^{-1} s^{-1} and indicates the onset of saturation of the sensors. Saturation will be further explained in Section 5.1. To allow for saturation of the sensor with higher mass fluxes, a Sigmoid curve was fitted to the data points. This regression does fit well with a correlation coefficient squared of 0.996 (Fig. 9, upper panel). Thereafter, the deviation of the measured data points from the predicted values was expressed in a percentage to determine the magnitude of variability in sensitivity of the sensors

$$s = \frac{|I_m - I_p|}{I_p} \cdot 100\%, \quad (4)$$

where s is the deviation of the measured value from the predicted value (%), I_m is the measured saltation intensity (counts s^{-1}) and I_p is the predicted value for saltation intensity (counts s^{-1}). The deviation of the measured values from the predicted values varies between 0.02 and 17.2% (Fig. 9, lower panel) with a dataset average (μ) and standard deviation (σ) of 4.91% and 4.14%, respectively. On average, the deviation decreases with increasing mass flux, and thus, the measured number of particles is more similar for individual sensors at higher saltation intensities. The magnitudes of the deviations ordered

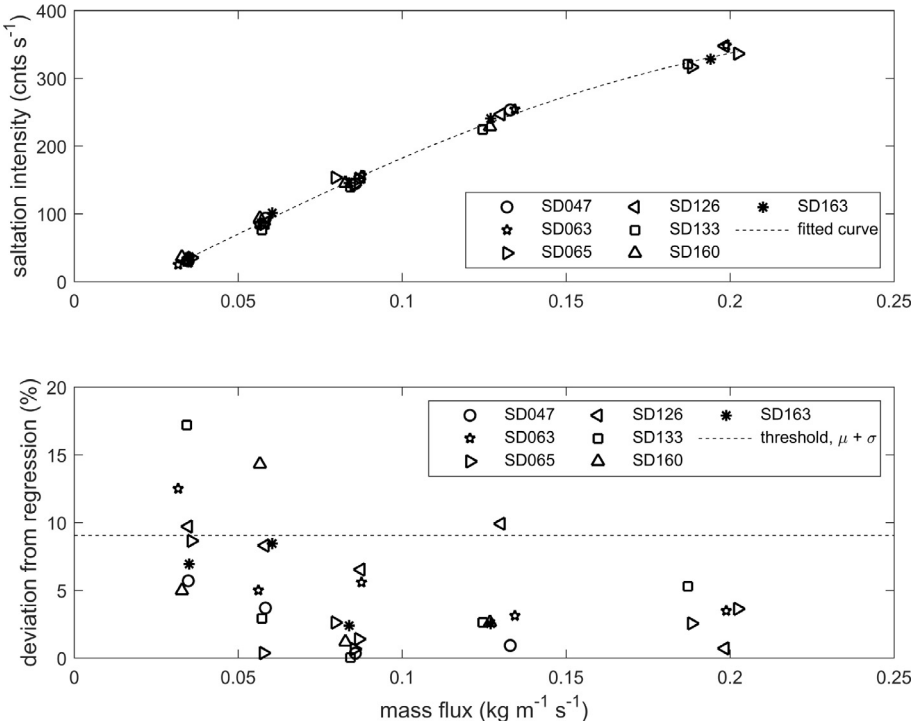

Fig. 9. Wind tunnel results. The upper panel shows the results of the wind tunnel experiments where every data point represents an experimental run with one single SalDec sensor (indicated by SD). The lower panel shows the deviation of the measured values from the values predicted with the Sigmoid curve fit.

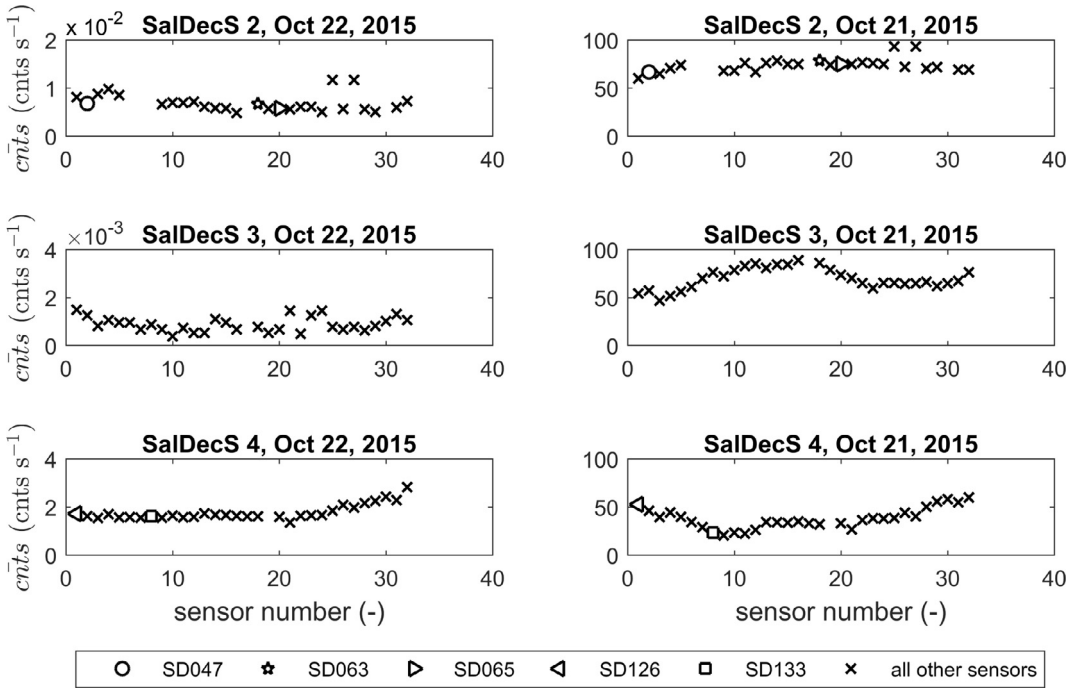

Fig. 10. Field experiment results of the 3 Saltation Detection Systems. The figures in the left column represent conditions with relatively small saltation intensities (October 22) compared to the figures in the right column (October 21). Note that the values for saltation intensity in the left column panels differ. The individual symbols (other than crosses) represent individual SalDec sensors tested during the wind tunnel experiments.

randomly for a given wind condition, as sensors were deployed in the same or reversed order. This suggests that differences are not caused by the experimental conditions or sensor sensitivity. Since the weighing accuracy is relatively small for small sediment losses from the sediment tray, increased deviations during little transport are most likely caused by effects of weighing accuracy. We assume that the large deviations during small mass fluxes are caused by the weighing accuracy rather than sensor sensitivity differences. As a rule of thumb, we use $\mu + \sigma$ as the threshold deviation of sensor sensitivity, which is 9%. Thus, if the outliers (> 9%) of the small mass fluxes are not taken into account and it is assumed that the weighing accuracy plays a role in the uncertainty of these mass fluxes, the deviations due to sensor sensitivity are below 9% from the predicted values.

4.2. Field experiments

Fig. 10 shows the results of the field experiments with three SalDecSs during relatively low (left column) and high (right column) saltation intensities. During relatively low saltation intensities the average saltation intensities increase with an order of magnitude from the sequence of SalDecS 2 up to SalDecS 4, whereas the high saltation intensities are in the same order of magnitude at every location across the beach. All conditions show wind-normal spatial variations in the time-averaged number of counts. These spatial variations can be subdivided into gradual and non-gradual variations. Gradual variations can be recognized by the sinusoidal wind-normal trend in, for example, the high intensity case measured with SalDecS 3 and 4. These gradual wind-normal variations are related to sand strips (Fig. 8, left photograph). These aeolian bed forms contain a sinusoidal alteration of bed surface height and soil moisture content, where the sand strips are elevated (in the order of centimeters) and drier compared to the adjacent surface area. Thus, the increased surface level combined with a smaller soil moisture content result in higher saltation intensities. Another case of gradual variability is observed for the low saltation intensity case of SalDecS 4. Here, the wind-normal trend increases toward the right end of the array. In the field, it was visually observed that this end deflected towards the surface, which thus explains higher saltation intensities at this part of the array.

Non-gradual wind-normal variabilities are visible at sensor 25 and 27 of SalDecS 2 and sensor 21 and 26 of SalDecS 4, in both the low and high saltation intensity cases. Sensor numbers 25 and 27 of SalDecS 2 show larger saltation intensity compared to the spatial trend over the horizontal array, suggesting a difference in sensor sensitivity, or a position slightly closer towards the bed surface. The time-averaged saltation intensity of sensor 25 and 27 is more than twice the magnitude of the average time-averaged saltation intensity of the two adjacent sensors during low intensity conditions. For high saltation intensity the deviations are about 27 and 31%. Sensor 21 and 26 of SalDecS 4 deviate from the spatial trend during both low (15.78 and 9.42%, respectively) and high (22.77 and 12.07%, respectively) saltation intensity. This might indicate a deviation in sensor sensitivity also, wherein sensor 21 would be less sensitive and sensor 26 more sensitive compared to the adjacent sensors. Additionally, the sensors of SalDecS 3 show an overall irregular spatial pattern during solely low saltation intensities. Because the deviating sensors of SalDecS 2 and 4 show inequalities with the adjacent sensors during both conditions, we can conclude that the inequality is structural and must be caused by an inequality of sensor sensitivity rather than morphological conditions. The irregular pattern of the horizontal array of SalDecS 3 is different from the individual deviations mentioned above, because these irregularities are not observed during high saltation intensities and thus are not structural. Besides, the low saltation intensity transport was visually observed to be non-continuous in space on temporal scales of seconds to minutes as only small clouds of sand were moving across the SalDecS array every now and then. This leads to occasionally and randomly spaced impacts of sand grains and thus the time-averaged spatial saltation intensity can show an irregular pattern. The irregular pattern can also be caused by the presence of small features such as footprints or beach debris. Since the spatial variation is gradual during high saltation intensity conditions and there are no corresponding spatial deviations in both situations, we can conclude that there are no sensors in SalDecS 3 that deviate because of sensitivity inequality.

5. Discussion

5.1. Non-linearity of SalDec sensors

Our wind tunnel results showed that saltation intensity is positively related to the mass flux. However, over the measured mass flux range, the relation is sigmoidal instead of linear. This indicates that at higher mass fluxes the sensor signal saturates and the increase in measured saltation intensity with mass flux thus decreases. During saturation the electronic signal is not translated into count pulses within the 1-ms interval of the signal shaper and the count signal of the hysteresis does not contain the transition of a 'grain' to 'no grain' (Section 2.2). The signal saturates when a large momentum is transferred to the sensor head which can be increased by impacts of large grains, high grain velocity and the intensity of the saltation process itself. A small grain with high velocity can exert the same momentum on the sensor head as a large grain with low velocity. Therefore, the point of saturation and thus the shape of the sigmoidal regression is dependent on the size and distribution of the grains in the sediment and their velocity. Because we used sand from our field site for the wind tunnel experiments, we can assume that there will be no differences in saturation characteristics in the field based on the influence of sediment size. Additional to the effect of grain size and velocity on saturation is the effect of high saltation intensity which causes a more continuous succession of grain impacts. During high saltation intensity, the probability of multiple sand grains hitting the sensor head at the same time or overlapping each-other is higher. Relatively high saltation intensities occur both during high wind velocities and closer to the bed surface. Thus, due to the latter aspect, the measuring height also influences the probability of sensor saturation and thus it is important that saltation intensity is not measured too close to the bed. However, the predominant saltation occurs within a layer with a thickness of about 0.1 m (Bagnold, 1941) and does not exceed the height of 0.5 m (Gillette et al., 1997), where the saltation layer thickness is dependent on particle diameter and wind speed (Gillette et al., 1997). Thus, to prevent sensor saturation, the measuring height cannot be too high as well because the predominant saltation decreases with height above the bed. It is thus important to use the minimum sensor height of 0.10 m (bottom of sensor head) in the field, since this measuring height results in only slight sensor saturation during the more extreme wind conditions as we have shown with our wind tunnel experiments. Even though the sensor height may influence the value of intermittency (Bauer and Davidson-Arnott, 2014; Sherman et al., 2017), mutual comparisons can still be done if the sensor height is constant.

Saturation was also empirically determined using the Wenglor laser sensor during fall flume experiments (Hugenholtz and Barchyn, 2011). They subdivide the response curve into a linear rising limb, a nonlinear region and a falling limb. Our windtunnel results also show a linear rising limb where the sensor response is positively related to the mass flux and the start of the nonlinear region. The falling limb is outside of our measuring range. To describe the saturation process of the SalDec sensor further, based on a simulation of the saltation process rather than falling sand grains, we developed an impact-response model (Appendix A). This model shows the three regions of the response curve identified by Hugenholtz and Barchyn (2011). Saturation of the sensor signal, described by the nonlinear region and the falling limb, where the sensor response is negatively related to the mass flux, raises the issue of the unreliability of point measurements due to flux ambiguity. As also pointed out by Hugenholtz and Barchyn (2011), a point measurement cannot be interpreted without additional data to support the substantiation whether a measurement is part of the rising or falling limb. To distinguish between a valid or saturated signal three types of data can be used. A sequence of data can be used to recognize the likely nature of the signal and to put the datapoints in a frame of reference. Second, our field setup contains a vertical array of sensors. These sensors measure the vertical saltation profile. If the number of particle counts increases towards the bed, the data are part of the rising limb. And finally, wind speed measurements can be used since our wind tunnel experiments showed the limit of at least 15.5 m s^{-1} (measured at 0.90 m above the bed) for severe saturation. During our field experiments observations with the vertical sensor array confirm that there was no significant influence of sensor saturation in the horizontal array since the time-averaged saltation intensity of the sensor just below 0.10 m showed an increasing trend towards the surface. Additionally, measured wind speeds were smaller than 9 m s^{-1} and are thus well below the limit of severe saturation.

Contrary to our measurements, Baas (2004) and Sterk et al. (1998) both found a linear relation between mass flux and saltation flux with the Safire and Saltiphone, respectively. Accordingly, they have not observed characteristics of sensor saturation. In the case of Baas (2004) it is hard to compare the results with our non-linear relation, because the linear relation of the Safire is based on sand fall flume experiments. Equally distributed falling sand grains is a different process than saltation. In the case of the Saltiphone the mass fluxes were in the same order of magnitude but in the upper range of our measurements from 0.17 to 0.30 kg m^{-2} s^{-1}, where our SalDec sensors start to saturate. This difference might be caused by grain size effects or the use of different construction material or experimental design. Raygosa-Barahona et al. (2016) found a linear relation of sensor counts depending on sediment weight in a fall flume experiment. However, just like the experiments in Sterk et al. (1998), only one single piezoelectric sensor was tested. So, the equality of sensor sensitivity could not be determined from their research.

5.2. Equality of SalDec sensor sensitivity

The wind tunnel results show a sensor variability of 9%. This indicates that variations in saltation intensity between sensors in the field less than the senor variability cannot be ascribed to the variability in the saltation process itself. Above this threshold, it is assumed that the sensitivity of the sensors is equal and that variability is caused by the saltation process.

Although it is difficult to quantify sensor deviation from our field data, we could make a distinction between non-gradual and gradual spatial variation. Non-gradual spatial variability was observed for 4 sensors out of a set of 89 working horizontally aligned sensors. The deviation of these sensors is likely caused by small errors in the standardized manufacture workflow. Therefore, it is requisite to apply such a workflow precisely to prevent sensitivity differences due to construction or material deviations. Gradual spatial variability likely indicates the presence of morphology-induced saltation variability, because in the field this occurs at the same spatial resolution and at the same location as sand strips. These gradual variable spatial patterns can thus be recognized in the data on temporal scales of the order of hours. All sensors which were filtered, based on a "no response" time series, were checked in the laboratory and defects with wiring or electronic connections were found, indicating that the sensors are fragile and need to be handled with care. However, the sensors did not show degradation like the Miniphone did after deployment in the field (Ellis et al., 2009).

The issue of sensor equality was only addressed by Baas (2004) to enable small scale variability investigation with the Safires. The Safires required normalization of the data along a sensor array because they have an unequal sensitivity to grain impacts. Here, we show that SalDec sensors have a mutually equal sensitivity with a threshold variability of 9% and thus these sensors are suitable to measure mutual differences in saltation intensity in the field without the need for signal normalization. Additionally, equal sensor sensitivity was not investigated for the piezoelectric sensor of Raygosa-Barahona et al. (2016).

6. Conclusions

We developed a low-cost Saltation Detection System that measures saltation intensity at a frequency of 10 Hz and on a spatial resolution of 0.10 m and a span of 3.1 m. Consistent with the predictions of a simple impact-response model, the output of the saltation sensors has a non-linear sigmoidal relation with the mass flux, illustrating increasing sensor saturation with increasing mass flux. Results of wind tunnel and field experiments were in the range of the positive (almost linear) relation between actual impacts (mass flux) and counted impacts (measured saltation intensity) which confirms that sensor saturation is not significant in our measurements. Based on wind tunnel experiments, the sensors have a variability in sensor sensitivity of about 9%. During field experiments, the sensors showed good equality as well, since only 4 of 89 horizontally deployed sensors deviated in sensor sensitivity. Therefore, we believe that the SalDecS can be used to measure relative saltation intensity using multiple sensors in the field. With the use of field measurements, the characteristics of the saltation process related to wind turbulence can be studied on small timescales (seconds) while on large timescales (hours) changes in morphological features (e.g., sand strip migration or small scale (centimeters) surface moisture characteristics) can be recognized.

Acknowledgements

We thank the two referees for their review and the various comments on the text. Wind tunnel and field experiments were performed with essential help of Yvonne Smit, Jasper Donker and Pam Hage. The research presented here was supported by the Dutch Technology Foundation STW (Vici project 13709), which is part of the Netherlands Organisation for Scientific Research (NWO), and which is partly funded by the Ministry of Economic Affairs.

Appendix A. Impact-response model

To examine saturation of a SalDec sensor, we developed a simple theoretical model that describes the relation between the actual number of impacts and the counted impacts for each second. Saltation intensity is represented by the actual number of particles that impact the sensor head and is set by an arbitrary number of sand particles, ranging from 100 to 2000 particles per second. The model calculates how often the signal of two successive sand grains overlaps for a certain saltation intensity. This is done using three timestamps: arrival time at the sensor head, pulse duration and the time when the signal has damped so that the sensor is ready to register a new sand grain. For the arrival time we assume that the saltation process is a random process through time and thus the simulated arrival time of each sand particle is random within the timeframe of 1 s. The pulse duration is calculated by:

$$D_{pulse} = D_{pulse,min} + w_{grainsize} * D_{extension,max}, \quad (5)$$

where D_{pulse} is the pulse duration (seconds), $D_{pulse,min}$ is the minimal pulse duration required to register a grain impact and is set to 0.0004 s, $w_{grainsize}$ is a weighing factor for grainsize (−) and $D_{extension,max}$ is the maximum pulse extension (s) (Table 3). The weighing factor is used to account for momentum variability caused by the variable grainsizes of the sediment. This factor is a random number between 0 and 1 and indicates the spectrum from small to large grains, respectively. The maximum pulse extension is linearly depending on saltation intensity and is thus also an arbitrary number in the same order of the minimum pulse duration. To calculate the timestamp when the signal has damped, we used:

$$T_{end} = T_{arrival} + D_{pulse}, \quad (6)$$

where T_{end} is the timestamp when the pulse has damped and $T_{arrival}$ is the arrival time (s) of a sand grain on the sensor head. The time the signal has damped is then compared to the arrival time and an overlap of sand grains is registered when the damping time of a grain is beyond the arrival time of the next grain. Then the number of counted impacts is determined by:

$$N_{counted} = N_{actual} - N_{overlap}, \quad (7)$$

where $N_{counted}$ is the number of counted impacts by the SalDec sensor, N_{actual} is the actual number of impacts on the sensor and $N_{overlap}$ is the number of overlapping sand grains.

The results of the model show that the probability of overlapping sand grains increases with saltation intensity (Fig. 11). This is clearly visible by the difference between the counted impats and the line of equality. The relation of the actual impacts and the counted impacts becomes even negative during saltation intensities with actual impacts in excess of 800 particles per second. When the amount of transport increases, the probability of overlapping sand grains increases as well and therefore, the grain count will be further and further postponed due to a longer signal damping. This causes a further decrease in the number of counted impacts when saltation intensity increases and the relation of the actual and counted impacts becomes negative. So although the model is based on arbitrary values, it does represent the process of signal registration.

Table 3
Maximum pulse extensions for saltation intensities.

Saltation intensity, actual impacts (−)	Maximum pulse extension (s)
100	0.0003
200	0.0004
300	0.0005
400	0.0006
500	0.0007
600	0.0008
800	0.0010
1000	0.0012
1200	0.0014
2000	0.0022

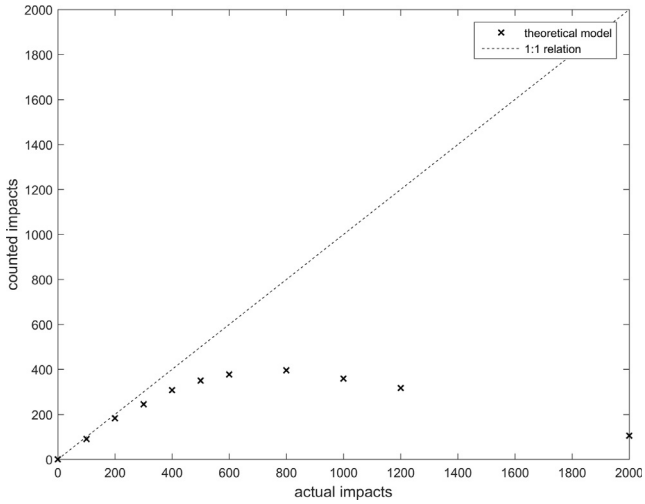

Fig. 11. Theoretical relation between the number of actual impacts and the number of counted impacts by the SalDec sensor for each second. Note that average impacts in the wind tunnel and field experiments remained below ~400 and ~100, respectively.

References

Baas, A.C.W., 2004. Evaluation of saltation flux impact responders (Safires) for measuring instantaneous aeolian sand transport intensity. Geomorphology 59, 99–118.

Baas, A.C.W., 2008. Challenges in aeolian geomorphology: investigating aeolian streamers. Geomorphology 93, 3–16.

Baas, A.C.W., Sherman, D.J., 2005. Foreffect and behavior of aeolian streamers. J. Geophys. Res. 110, F03011.

Baas, A.C.W., Sherman, D.J., 2006. Spatiotemporal variability of aeolian sand transport in a coastal dune environment. J. Coastal Res. 22 (5), 1198–1205.

Bagnold, R.A., 1941. The Physics of Blown Sand and Desert Dunes. Methuen & Co. LTD, London.

Barchyn, T.E., Hugenholtz, C.H., 2010. Field comparison of four piezoelectric sensors for detecting aeolian sediment transport. Geomorphology 120, 368–371.

Barchyn, T.E., Hugenholtz, C.H., Li, B., Neuman, C.M., Sanderson, R.S., 2014. From particle counts to flux: Wind tunnel testing and calibration of the 'Wenglor' aeolian sediment transport sensor. Aeolian Res. 15, 311–318.

Barchyn, T.E., Martin, R.L., Kok, J.F., Hugenholtz, C.H., 2014. Fundamental mismatches between measurements and models in aeolian sediment transport prediction: the role of small scale variability. Aeolian Res. 15, 245–251.

Bauer, B.O., Davidson-Arnott, R.G.D., 2014. Aeolian particle flux profiles and transport unsteadiness. J. Geophys. Res.: Earth Surface 119, 1542–1563.

Davidson-Arnott, R.G.D., Bauer, B.O., 2009. Aeolian sediment transport on a beach: thresholds, intermittency, and high frequency variability. Geomorphology 105, 117–126.

Davidson-Arnott, R.G.D., Law, M.N., 1996. Measurements and prediction of long-term sediment supply to coastal foredunes. J. Coastal Res. 12, 654–663.

de Winter, R.C., Gongriep, F., Ruessink, B.G., 2015. Observations and modeling of alongshore variability in dune erosion at Egmond aan Zee, the Netherlands. Coast. Eng. 99, 167–175.

Duarte-Campos, L., Wijnberg, K.M., Oyarte-Gálvez, L., Hulscher, S.J.M.H., 2017. Laser particle counter validation for aeolian sand transport measurements using a high-speed camera. Aeolian Res. 25, 37–44.

Durán, O., Moore, L., 2013. Vegetation controls on the maximum size of coastal dunes. Proc. Nat. Acad. Sci. 110 (43), 17217–17222.

Ellis, J.T., Morrison, R.F., Priest, B.H., 2009. Detecting impacts of sand grains with a microphone system in field conditions. Geomorphology 105, 87–94.

Gabriels, D., Cornelis, W., Pollet, I., Coillie, T.V., Ouessar, M., 1997. The I.C.E. wind tunnel for wind and water erosion studies. Soil Technol. 10, 1–8.

Gillette, D.A., Fryrear, D.W., Xiao, J.B., Stockton, P., Ono, D., Helm, P.J., Gill, T.E., Ley, T., 1997. Large-scale variability of wind erosion mass flux rates at owens lake: 1. Vertical profiles of horizontal mass fluxes of wind-eroded particle with diameter greater than 50 micrometer. J. Geophys. Res. 102, 25977–25987.

Hage, P., Ruessink, G., Donker, J., under review. Determining sand strip characteristics using video monitoring. Aeolian Res.

Holman, R.A., Stanley, J., 2007. The history and technical capabilities of Argus. Coast. Eng. 54, 477–491.

Hsu, S.A., 1971. Wind stress criteria in eolian sand transport. J. Geophys. Res. 76, 8684–8686.

Hugenholtz, C.H., Barchyn, T.E., 2011. Laboratory and field performance of a laser particle counter for measuring aeolian sand transport. J. Geophys. Res. 116, F01010.

Kadib, A.A., 1965. A function for sand movement by wind. Hydraulics Engineering Laboratory Report HEL 2–8, UCLA-Berkeley. University of California, Berkeley, CA.

Kawamura, R., 1951. Study of sand movement by wind. Rep. Inst. Sci. Technol. 5, 95–112.

Keijsers, J.G.S., de Groot, A.V., Riksen, M.J.P.M., 2016. Modeling the biogeomorphic evolution of coastal dunes in response to climate change. J. Geophys. Res.: Earth Surface 121, 1161–1181.

Keijsers, J.G.S., Poortinga, A., Riksen, M.J.P.M., Maroulis, J., 2014. Spatio-temporal variability in accretion and erosion of coastal foredunes in the Netherlands: Regional climate and local topography. PLOS ONE 9.

Kobayashi, N., Buck, M., Payo, A., Johnson, B.D., 2009. Berm and dune erosion during a storm. J. Waterway Port Coastal Ocean Eng. 135, 1–10.

Lee, Z.S., Baas, A.C.W., 2015. Variable and conflicting shear stress estimates inside a boundary layer with sediment transport. Earth Surf. Proc. Land. 41 (4), 435–445.

Leenders, J.K., van Boxel, J.H., Sterk, G., 2005. Wind forces and related saltation transport. Geomorphology 71, 357–372.

Lettau, K., Lettau, H., 1978. Exploring the World's Driest Climate. IES Report 101. Center for Climatic Research, University of Wisconsin-Madison, Ch. Experimental and micrometeorological field studies of dune migration, pp. 110–147.

Nield, J.M., Wiggs, G.F.S., Squirrell, R.S., 2011. Aeolian sand strip mobility and protodune development on a drying beach: examining surface moisture and surface roughness patterns measured by terrestrial laser scanning. Earth Surf. Proc. Land. 36, 513–522.

Owen, P.R., 1964. Saltation of uniform grains in air. J. Fluid Mech. 20, 225–242.

Poortinga, A., van Rheenen, H., Ellis, J.T., Sherman, D.J., 2015. Measuring aeolian sand transport using acoustic sensors. Aeolian Res. 16, 143–151.

Raygosa-Barahona, R., Ruiz-Martinez, G., Mariño-Tapia, I., Heyser-Ojeda, E., 2016. Design and initial testing of a piezoelectric sensor to quantify aeolian sand transport. Aeolian Res. 22, 127–134.

Roelvink, D., Reniers, A., van Dongeren, A., van Thiel de Vries, J., McCall, R., Lescinski, J., 2009. Modelling storm impacts on beaches, dunes and barrier islands. Coast. Eng. 56, 1133–1152.

Ruessink, B.G., Boers, M., van Geer, P.F.C., de Bakker, A.T.M., Pieterse, A., Grasso, F., de Winter, R.C., 2012. Towards a process-based model to predict dune erosion along the Dutch Wadden coast. Neth. J. Geosci. 91, 357–372.

Sherman, D.J., Li, B., 2012. Predicting aeolian sand transport rates: a re-evaluation of models. Aeolian Res. 3, 371–378.

Sherman, D.J., Li, B., Farrell, E.J., Ellis, J.T., Cox, W.D., Maia, L.P., Sousa, P.H.G.O., 2011. Measuring aeolian saltation: a comparison of sensors. J. Coast. Res. SI59, 280–290.

Sherman, D.J., Li, B., Ellis, J.T., Swann, C., 2017. Intermittent aeolian saltation: a protocol for quantification. Geogr. Rev. 1–19.

Sorensen, M., 2004. On the rate of aeolian sand transport. Geomorphology 59, 53–62.

Spaan, W.P., van den Abeele, G.D., 1991. Wind borne particle measurements with acoustic sensors. Soil Technol. 4, 51–63.

Sterk, G., Jacobs, A.F.G., van Boxel, J.H., 1998. The effect of turbulent flow structures on saltation sand transport in the atmospheric boundary layer. Earth Surf. Proc. Land. 23, 877–887.

Stockton, P.H., Gillette, D.A., 1990. Field measurement of the sheltering effect of vegetation on erodible land surfaces. Land Degrad. Rehabil. 2, 77–85.

Stout, J.E., Zobeck, T.M., 1997. Intermittent saltation. Sedimentology 44, 959–970.

Thornton, E.B., MacMahan, J., Sallenger, A.H., 2007. Rip currents, mega-cusps, and eroding dunes. Mar. Geol. 240, 151–167.

van Enckevort, I.M.J., Ruessink, B.G., 2001. Effect of hydrodynamics and bathymetry on video estimates of nearshore sandbar position. J. Geophys. Res. 106 (C8), 16969–16979.

Vellinga, P., 1982. Beach and dune erosion during storm surges. Coast. Eng. 6, 361–387.

Zingg, A.W., 1953. Wind tunnel studies of the movement of sedimentary material. In: Proceedings, 5th Hydraulics Conference, Studies in Engineering. vol. 34. pp. 111–135.